Additional methodological details

P-T pseudosection calculation

To constrain detailed P-T paths of the garnet-micaschists and the garnet-kyanite-micaschists, pseudosections were calculated in the NCKFMASHT-system, using the THERIAK-DOMINO software (v. 20/03/07) of De Capitani and Brown (1987), with the internally consistent thermodynamic dataset of Holland and Powell (1998) (THERIAK-DOMINO filename tcdb55c2d.txt) and the mineral activity models of Baldwin et al. (2005) for feldspar, White et al. (2007) for garnet, biotite, and ilmenite, and liquid, Holland and Powell (1998) for cordierite, Holland and Powell (1996) for clinopyroxene, and Coggon and Holland (2002) for white mica. The chemistry of both the garnet-micaschists and the garnet-kyanite-micaschists is adequately expressed in the system NCKFMASHT system as additional components are only present at trace element level and will thus not significantly affect the topology of the pseudosections. Water contents are directly taken from the determined LOI. In order to refine the estimation of the peak conditions we have calculated isopleths for the X_{Mg} (calculated as molar Mg/(Mg+Fe)) and X_{Grs} (calculated as molar Ca/(Ca+Mg+Fe) of garnet, the X_{Cel} (molar celadonite component, calculated as molar Mg-celadonite/(Mg-celadonite+Fe-celadonite+paragonite+muscovite) of white mica, X_{An} (molar anorthite component, calculated as molar Ca/(Ca+Na+K) of plagioclase, and the X_{Mg} of biotite. Mineral phases from samples 070a and MF4 were analysed by a JEOL JXA 8530F electron microprobe with a field-emitting cathode at the Institute for Micro Process Engineering at the Karlsruhe Institute of Technology (KIT). Representative analyses are shown in Tables DR2.1, 2.2., 2.3, 2.4.

Rb-Sr- and Sm-Nd-multimineral geochronology

Deformation-induced recrystallization of white mica and associated phases will generally lead to complete Sr-isotopic re-equilibration and reset of ages (Müller et al., 1999). Such reset ages date the last recrystallization-inducing process, i.e. the waning stages of deformation (Freeman et al., 1998) provided that no later thermal-diffusive or retrogressive overprint occurred. Diffusional resetting of the Rb-Sr system in white mica is activated only at amphibolite facies temperatures >550°C (cf. Villa, 1998). At fluid-absent conditions, age signatures can persist through even higher temperatures (>600°C) on orogenic time scales (Glodny et al., 2008a). Any protracted diffusional resetting would leave a distinctive signature in the mica population, namely a correlation between apparent age and grain size (Glodny et al., 2008b). We therefore analyzed

white mica in different grain size fractions, both to check for a possible presence of mixed mica populations, i.e. of unequilibrated, pre-deformational white mica relics (cf. Müller et al., 1999), and to distinguish between deformation-induced and diffusion-induced isotopic resetting.

Isotopic data were generated at GFZ Potsdam using a Thermo Scientific TRITON thermal ionization mass spectrometer. Sr and Nd were measured in dynamic multicollection mode, Rb and Sm in static multicollection mode. The values obtained for isotopic standards during the period of analytical work were 0.710255 ± 0.000005 (n = 23) for $^{87}Sr/^{86}Sr$ in the SRM 987 and 0.511850 ±0.000004 (n = 7) for $^{143}Nd/^{144}Nd$ in the La Jolla Nd standard, respectively. For age calculation, standard errors of ±0.003% for $^{143}Nd/^{144}Nd$ ratios, of ±0.5% for $^{147}Sm/^{144}Nd$ ratios, of ±0.005% for $^{87}Sr/^{86}Sr$ and of ±1.5% for $^{87}Rb/^{86}Sr$ ratios were assigned to the results. Handling of mineral separates and analytical procedures are described in Glodny et al. (2008a,b,c). Uncertainties of isotope and age data are quoted at 2σ throughout this work. The program ISOPLOT/EX 3.71 (Ludwig, 2009) was used to calculate regression lines. Decay constants are those recommended by Steiger and Jäger (1977).

References cited

Baldwin, J.A., Powell, R., Brown, M., Moraes, R. and Fuck, R.A., 2005. Modelling of mineral equilibria in ultrahigh-temperature metamorphic rocks from the Anapolis-Itaucu Complex, central Brazil: Journal of metamorphic Geology, v. 23, no. 7, p. 511-531.

Coggon, R. and Holland, T.J.B., 2002. Mixing properties of phengitic micas and revised garnet-phengite thermobarometers: Journal of metamorphic Geology, v. 20, no. 7, p. 683-696.

De Capitani, C. and Brown, T.H., 1987. The computation of chemical equilibrium in complex systems containing non-ideal solutions: Geochimica et Cosmochimica Acta, v. 51, p. 2639-2652.

Freeman, S.R., Butler, R.W.H., Cliff, R.A. and Rex, D.C., 1998. Direct dating of mylonite evolution: A multi-disciplinary geochronological study from the Moine Thrust Zone, NW Scotland: Journal of the Geological Society, v. 155, no. 5, p. 745-758.

Glodny, J., Kühn, A. and Austrheim 2008a. Geochronology of fluid-induced eclogite and amphibolite facies metamorphic reactions in a subduction–collision system, Bergen Arcs, Norway: Contributions to Mineralogy and Petrology, v. 156, p. 27–48.

Glodny, J., Kühn, A. and Austrheim, H., 2008b. Diffusion versus recrystallization processes in Rb–Sr geochronology: Isotopic relics in eclogite facies rocks, Western Gneiss Region, Norway: Geochimica et Cosmochimica Acta, v. 72, p. 506-525.

Glodny. J., Ring, U. and Kühn. A., 2008c. Coeval high-pressure metamorphism, thrusting, strike-slip, and extensional shearing in the Tauern Window, Eastern Alps: Tectonics, v. 27, TC4004.

Holland, T.J.B. and Powell, R., 1996. Thermodynamics of order-disorder in minerals; II, Symmetric formalism applied to solid solutions: American Mineralogist, v. 81, p. 1425-1437.

Holland, T.J.B. and Powell. R., 1998. An internally consistent thermodynamic data set for phases of petrological interest: Journal of metamorphic Petrology, v. 16, p. 309-343.

Ludwig, K., 2009. Isoplot v. 3.71: A geochronological toolkit for Microsoft Excel: Berkeley, California: Berkeley Geochronology Center, Special Publication, v. 4, 70 p.

Müller, W., Dallmeyer, R.D., Neubauer, F. and Thöni, M., 1999. Deformation-induced resetting of Rb/Sr and $^{40}Ar/^{39}Ar$ mineral systems in a low-grade, polymetamorphic terrane (Eastern Alps Austria): Journal of the Geological Society, London, v. 156, p. 261-278.

Steiger, R. H. and Jäger, E., 1977. Subcommission on geochronology: Convention on the use of decay constants in geo- and cosmochronology: Earth and Planetary Science Letters, v. 36, p. 359-362.

White, R.W., Powell, R., Holland, T.J.B., 2007. Progress relating to calculation of partial melting equilibria for metapelites: Journal of metamorphic Geology, v. 25, no. 5, p. 511–527.

Villa, I.M., 1998. Isotopic closure. Terra Nova v. 10, no. 1, p. 42-47

Table DR1: Sample locations.

Sample	N-latitude	E-longitude
MF3	65°04,970´	15°20,225´
MF4	65°02,824´	15°21,514´
VAK	64°40,365´	14°20,189´
070a	65°00,878´	14°41,900´
120a	64°58,967´	14°41,628´
131a	65°00,892´	14°38,607´
155a	64°58,895´	14°41,710´

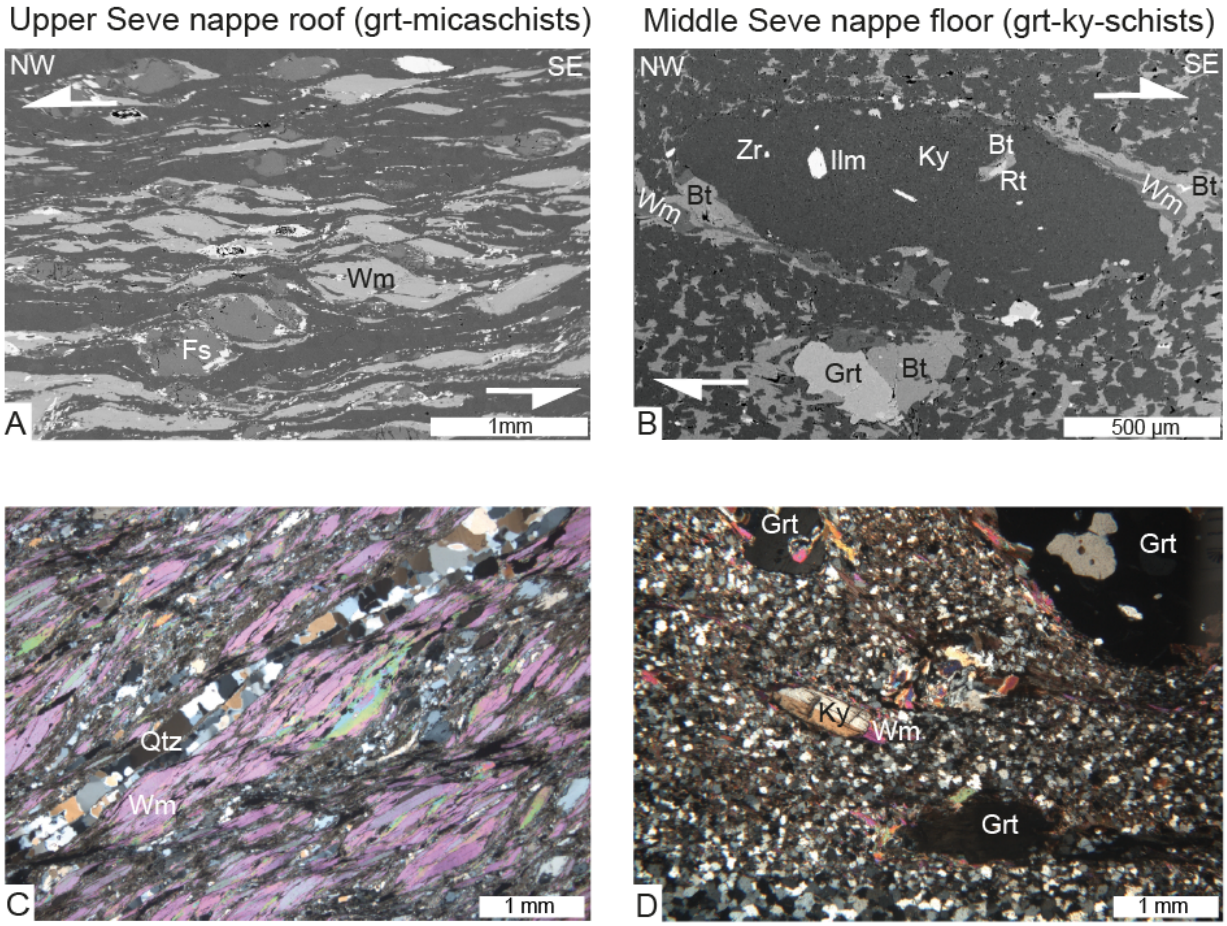

Figure DR1: A, B) SEM-images (xz-sections) of representative samples showing asymmetric kinematic indicators with opposing shear senses for Upper Seve nappe roof (A) and Middle Seve nappe floor (B) shear zones (Fs: feldspar, Wm: white mica). C) Thin section images of garnet micaschists from the Upper Seve nappe roof (sample 070a) and D) garnet-kyanite micaschists from the Middle Seve nappe floor (sample MF4) shear zones. A, C) Quartz (Qtz) recrystallized at small grain sizes <10 µm in the matrix, but form larger grains in up to 500 µm thick quartz ribbons. These quartz ribbons show pinch-and-swell along developing high-angle C´-type synthetic shear bands cutting across the mylonitic S-C-fabric. B, D) A very fine-grained micaceous-quartzitic matrix contains rotated porphyroclasts of (commonly) twinned kyanite (Ky) and garnet (Grt) with asymmetric recrystallization tails consisting of white mica (Wm) and biotite (Bt) around kyanite and of biotite around garnet (Grt) indicating top-to-SE sense of shear. Inclusions in garnet are >200 µm large quartz and small biotite. Inclusions in kyanite are ilmenite (Ilm), rutile (Rt), zircon (Zr), and biotite (Bt).

Table DR2.1: Selected electron microprobe analyses of garnet in samples MF4 and 070a.

Sample No./Position	MF4 1.00	MF4 2.00	MF4 6.00	MF4 7.00	MF4 8.00	MF4 9.00	070a core	070a rim
SiO_2	39.31	38.81	37.83	38.06	38.88	38.90	38.37	38.28
TiO2	0.02	0.02	0.00	0.00	0.00	0.01	0.08	0.07
Al_2O_3	22.76	22.21	22.10	21.87	22.47	22.22	21.43	21.63
Cr_2O_3	0.00	0.00	0.00	0.00	0.00	0.00	0.02	0.03
Fe_2O_3	0.00	0.00	0.00	0.00	0.00	0.00	0.00	0.00
MgO	7.24	4.65	4.38	4.30	5.13	4.19	2.17	2.26
CaO	2.70	2.79	2.77	2.58	2.95	2.82	6.45	6.92
MnO	1.37	3.12	3.33	3.45	1.94	3.60	6.72	4.73
FeO	28.42	30.35	30.47	30.46	30.39	30.34	26.49	27.74
Na_2O	0.00	0.02	0.05	0.05	0.01	0.03	0.02	0.01
Sum	**101.82**	**101.97**	**100.92**	**100.77**	**101.77**	**102.10**	**101.75**	**101.67**
Formula (O=24)								
Si	5.99	6.02	5.95	5.99	6.01	6.03	6.03	6.01
$Al^{(4)}$	0.01	0.00	0.05	0.01	0.00	0.00	0.00	0.00
Sum	**6.00**	**6.02**	**6.00**	**6.00**	**6.01**	**6.03**	**6.03**	**6.01**
Fe^{3+}	0.00	0.00	0.00	0.00	0.00	0.00	0.00	0.00
$Al^{(6)}$	4.08	4.05	4.05	4.05	4.09	4.06	4.02	4.02
Sum	**4.08**	**4.05**	**4.05**	**4.05**	**4.09**	**4.06**	**4.02**	**4.01**
Ti	0.00	0.00	0.00	0.00	0.00	0.00	0.01	0.01
Na	0.00	0.01	0.01	0.01	0.00	0.01	0.01	0.00
Mg	1.64	1.07	1.03	1.01	1.18	0.97	0.51	0.53
Ca	0.44	0.46	0.47	0.44	0.49	0.47	1.09	1.16
Mn	0.18	0.41	0.44	0.46	0.25	0.47	0.89	0.63
Fe^{2+}	3.62	3.93	4.01	4.01	3.93	3.93	3.48	3.64
Sum	**5.88**	**5.89**	**5.96**	**5.93**	**5.85**	**5.85**	**5.98**	**5.97**
Sum cations	**15.96**	**15.96**	**16.01**	**15.98**	**15.95**	**15.94**	**16.03**	**15.99**
Andradite	0.00	0.00	0.00	0.00	0.00	0.00	0.00	0.00
Grossular	7.49	7.87	7.86	7.37	8.35	8.01	18.19	19.52
Almandine	61.55	66.89	67.42	67.80	67.13	67.32	58.31	61.07
Spessartine	3.01	6.96	7.45	7.78	4.33	8.10	14.98	10.55
Pyrope	27.95	18.28	17.27	17.06	20.19	16.57	8.52	8.87
X_{Mg}	0.31	0.21	0.20	0.20	0.23	0.20	0.13	0.13

Table DR2.2: Selected electron microprobe analyses of biotite in samples MF4 and 070a.

Sample	MF4	MF4	MF4	MF4	MF4	070a
Point	10	11	13	4	5	1
Position	incl. in grt	foliation	foliation	around grt	around grt	foliation
SiO_2	36.81	37.04	35.94	35.40	35.81	36.78
TiO_2	1.93	3.13	3.44	3.35	3.32	2.64
Al_2O_3	18.25	17.82	17.32	16.97	17.29	16.50
FeO	17.61	17.79	18.67	19.58	19.05	19.29
MnO	0.04	0.06	0.06	0.04	0.05	0.09
MgO	11.14	10.62	10.42	9.83	9.73	10.32
CaO	0.02	0.01	0.03	0.00	0.00	0.01
Na_2O	0.17	0.17	0.10	0.13	0.15	0.05
K_2O	9.23	9.54	9.38	9.33	9.50	9.69
Cl	0.27	0.30	0.36	0.40	0.33	n.d.
Total	**95.46**	**96.48**	**95.72**	**95.01**	**95.21**	**95.43**
Formula (O,OH,F=22)						
Si^{IV}	5.53	5.52	5.44	5.43	5.47	5.60
Al^{IV}	2.47	2.48	2.56	2.57	2.53	2.40
Ti^{IV}	0.00	0.00	0.00	0.00	0.00	0.00
Sum T	**8.00**	**8.00**	**8.00**	**8.00**	**8.00**	**8.00**
Al^{VI}	0.76	0.65	0.53	0.50	0.58	0.55
Ti^{VI}	0.22	0.35	0.39	0.39	0.38	0.30
Fe	2.21	2.22	2.36	2.51	2.43	2.45
Mg	2.49	2.36	2.35	2.25	2.21	2.34
Mn	0.00	0.01	0.01	0.00	0.01	0.01
Sum VI	**5.69**	**5.59**	**5.65**	**5.66**	**5.61**	**5.67**
Ca	0.00	0.00	0.00	0.00	0.00	0.00
Na	0.05	0.05	0.03	0.04	0.04	0.01
K	1.77	1.81	1.81	1.83	1.85	1.88
Sum XII	**1.82**	**1.87**	**1.85**	**1.86**	**1.89**	**1.90**
Cl	0.07	0.08	0.09	0.10	0.08	n.d.
Sum anions	0.07	0.08	0.09	0.10	0.08	n.d.
Sum cations	**15.51**	**15.46**	**15.50**	**15.52**	**15.50**	**15.57**
X_{Mg}	0.53	0.52	0.50	0.47	0.48	0.49

n.d.: not determined

Table DR2.3: Selected electron microprobe analyses of white mica in samples MF4 and 070a.

Sample No.	MF4 3	MF4 12	MF4 14	070a 2 (1µm)	070a 3 (3µm)
SiO_2	45.98	46.36	46.38	46.26	46.65
TiO_2	0.98	1.07	1.31	0.76	0.77
Al_2O_3	32.05	32.66	31.10	31.61	31.94
FeO	3.09	2.91	2.78	4.04	4.14
MnO	0.00	0.00	0.01	0.01	0.00
MgO	1.18	0.99	1.39	1.21	1.21
CaO	0.00	0.00	0.04	0.00	0.00
Na_2O	0.54	0.52	0.59	0.69	0.72
K_2O	10.29	10.41	10.29	10.36	10.07
Cl	0.02	0.01	0.03	n.d.	n.d.
Total	**94.15**	**94.92**	**93.92**	**94.98**	**95.55**
Formula (O,OH,F=22)					
Si^{IV}	6.26	6.25	6.32	6.28	6.28
Al^{IV}	1.74	1.75	1.68	1.72	1.72
Ti^{IV}	0.00	0.00	0.00	0.00	0.00
Sum T	**8.00**	**8.00**	**8.00**	**8.00**	**8.00**
Al^{VI}	3.41	3.44	3.32	3.34	3.35
Ti^{VI}	0.10	0.11	0.13	0.08	0.08
Fe	0.35	0.33	0.32	0.46	0.47
Mg	0.24	0.20	0.28	0.24	0.24
Mn	0.00	0.00	0.00	0.00	0.00
Sum VI	**4.10**	**4.08**	**4.06**	**4.12**	**4.14**
Ca	0.00	0.00	0.01	0.00	0.00
Na	0.14	0.13	0.16	0.18	0.19
K	1.79	1.79	1.79	1.79	1.73
Sum XII	**1.93**	**1.93**	**1.95**	**1.98**	**1.92**
Sum cations	14.03	14.00	14.01	14.10	14.06
Paragonite	7.44	6.99	7.96	9.19	9.80
Celadonite	12.40	10.38	14.52	12.39	12.67
Muscovite	61.93	65.58	60.97	55.20	53.22
Fe-Celadonite	18.22	17.02	16.21	23.22	24.31
Margarite	0.02	0.03	0.33	0.00	0.00

n.d.: not determined

Table DR2.4: Selected electron microprobe analyses of plagioclase in samples MF4 and 070a

Sample	MF4	MF4	070a	070a
Position	core	core	core	rim
SiO_2	65.07	64.70	60.60	63.60
TiO_2	0.00	0.00	0.00	0.00
Al_2O_3	22.68	22.15	25.18	23.89
MgO	0.00	0.00	0.01	0.00
CaO	3.30	3.38	6.63	4.75
MnO	0.00	0.00	0.01	0.02
Fe_2O_3	0.17	0.17	0.16	0.12
BaO	0.00	0.00	0.00	0.00
Na_2O	8.97	9.60	7.88	8.95
K_2O	0.15	0.12	0.12	0.08
Sum	**100.34**	**100.12**	**100.59**	**101.41**
Formula (O=8)				
Si	2.85	2.85	2.68	2.77
Al^{VI}	1.17	1.15	1.31	1.23
Ti	0.00	0.00	0.00	0.00
Mg	0.00	0.00	0.00	0.00
Ca	0.15	0.16	0.31	0.22
Mn	0.00	0.00	0.00	0.00
Fe^{3+}	0.01	0.01	0.01	0.00
Ba	0.00	0.00	0.00	0.00
Na	0.76	0.82	0.68	0.76
K	0.01	0.01	0.01	0.00
Sum	**4.95**	**4.99**	**5.00**	**4.99**
Anorthite	16.74	16.18	31.52	22.57
Albite	82.35	83.14	67.80	76.97
Orthoclase	0.91	0.68	0.68	0.45
Celsian	0.00	0.00	0.00	0.00

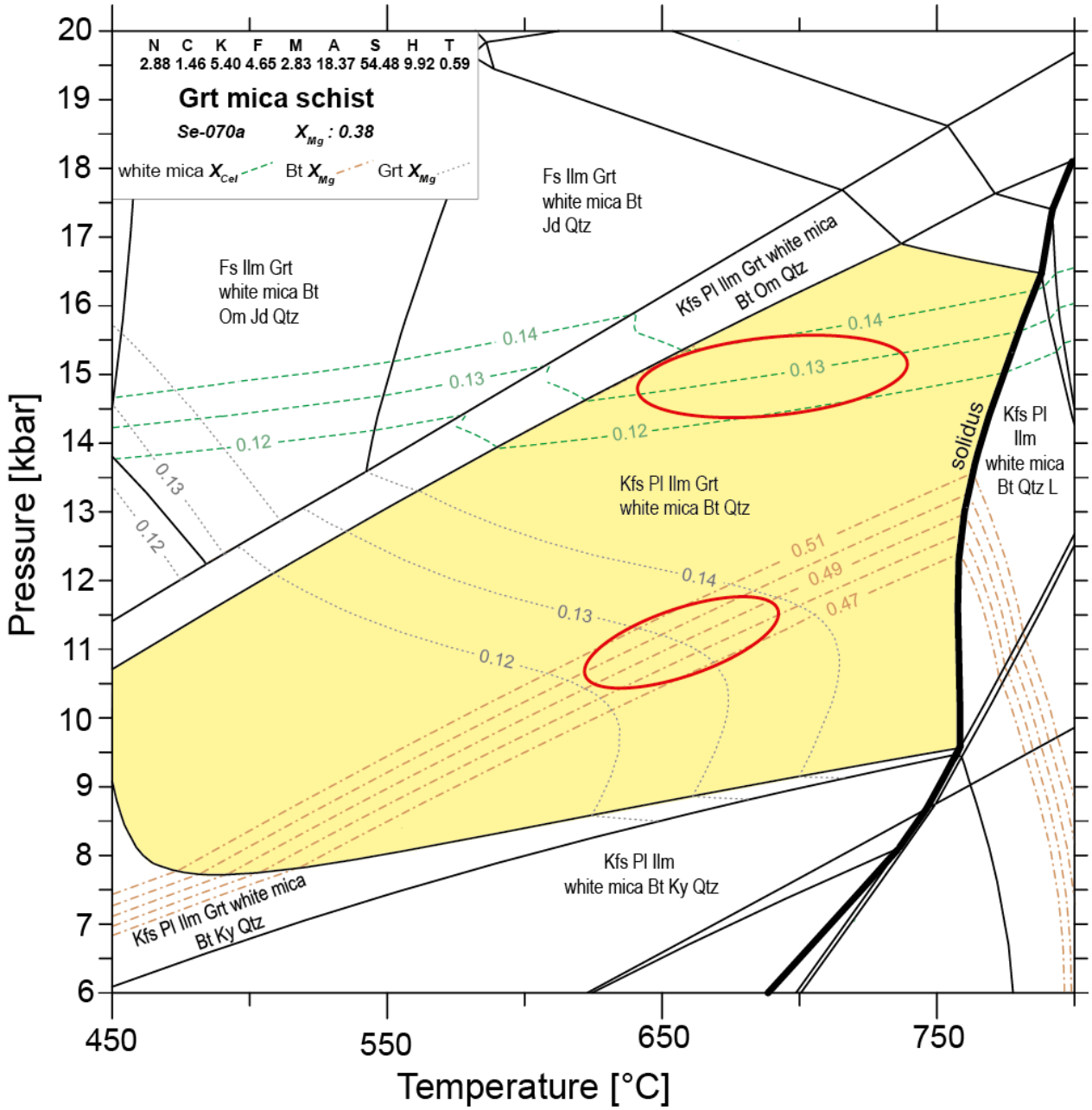

Figure DR2a: Detailed PT-pseudosection of Upper Seve nappe roof shear zone (sample 070a) showing stability fields at the given NCKFMASHT-system at 450 to 800 °C and 6 to 20 kbar. The solidus is highligthed by a bold line. Yellow-shaded stability field highlights observed paragenesis. Ellipses highlight PT-arrays in the stability field as constrained by intersection of isopleths derived from the Mg-content in garnet (X_{Mg}), the celadonite content in white mica (X_{cel}), the Mg-content of biotite, and (not shown) the grossular content of garnet (X_{Grs}). Rt - rutile, Grt - garnet, Bt - biotite, Fs - feldspar, Ilm - ilmenite, Ky - kyanite, Qtz - quartz, Pl - plagioclase, Kfs: K-feldspar, Om - omphacite, Jd – jadeite, L - liquid.

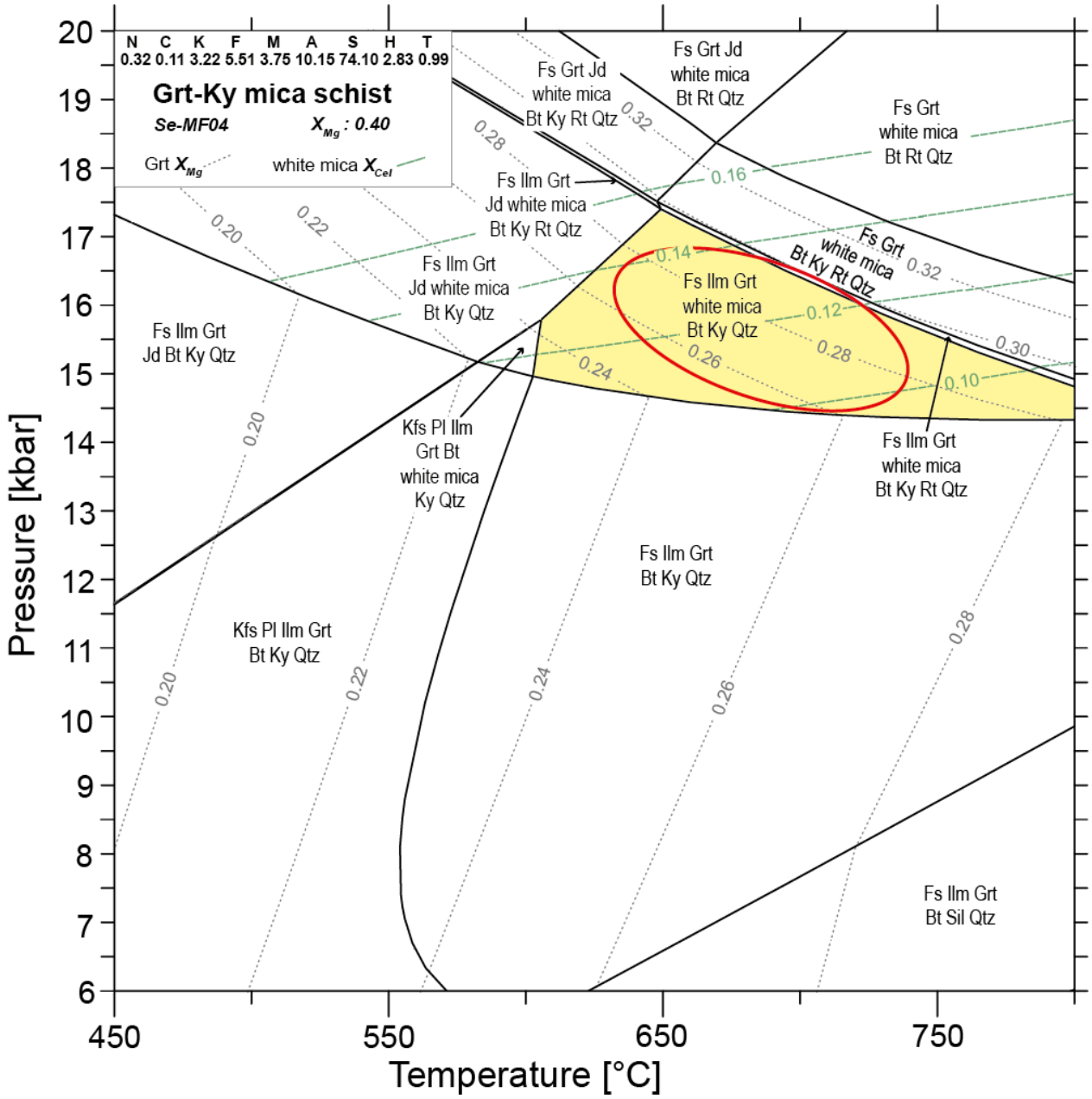

Figure DR2b: Detailed PT-pseudosection of Middle Seve nappe floor shear zone (sample MF4) showing stability fields at the given NCKFMASHT-system at 450 to 800 °C and 6 to 20 kbar. Yellow shaded stability field highlights observed paragenesis. Ellipse highlights PT-array as constrained by intersection of isopleths derived from the Mg-content in garnet (X_{Mg}), the celadonite content in white mica (X_{Cel}), and (not shown) the anorthite content of plagioclase and Mg-content of biotite. Rt - rutile, Grt - garnet, WM - white mica, Bt - biotite, Fs - feldspar, Ilm - ilmenite, Ky - kyanite, Sil - sillimanite, Qtz - quartz, Pl - plagioclase, Kfs - K-feldspar, Jd - jadeite.

Table DR3.1: Detailed Rb-Sr-isotope data.

Sample no. Analysis no.	Material	Rb (ppm)	Sr (ppm)	$^{87}Rb/^{86}Sr$	$^{87}Sr/^{86}Sr$	$^{87}Sr/^{86}Sr$ $2\sigma_m$ [%]
120a (micaschist; 431.0 ± 8.9 Ma; Sr_i = 0.7395 ± 0.0010; MSWD = 720; n = 8)						
430.7 ± 9.5 Ma; Sr_i = 0.7396 ± 0.0012; MSWD = 859; n = 7 (excl. relic garnet)						
PS1747	quartz-feldspar	4.88	197	0.0721	0.740739	0.0014
PS1752	wm 160-125 µm	260	75.1	10.1	0.801596	0.0015
PS1751	wm 250-160 µm	285	61.8	13.5	0.821694	0.0028
PS1750	wm 355-250 µm	284	61.3	13.5	0.821966	0.0009
PS1749	wm 500-355 µm	277	61.0	13.3	0.822328	0.0011
PS1748	Apatite	2.41	383	0.0183	0.738680	0.0014
PS1745	whole rock	109	151	2.10	0.752827	0.0009
PS1746	Garnet	1.24	0.77	4.68	0.767588	0.0090
155a (mylonit. micaschist; 438.4 ± 3.2 Ma; Sr_i = 0.732661 ± 0.00036; MSWD = 0.9, n = 5 (recryst. phases)						
494 ± 66 Ma; Sr_i = 0.7267 ± 0.0054; MSWD = 41361, n = 9 (all data)						
PS1761	quartz-feldspar	3.75	263	0.0416	0.732921	0.0008
PS1760	wm 160-125 µm	231	98.7	6.81	0.774903	0.0006
PS1759	wm 250-160 µm	244	87.9	8.08	0.782829	0.0011
PS1758	wm 355-250 µm	239	83.6	8.32	0.784950	0.0026
PS1757	wm 500-355 µm	241	81.3	8.66	0.787056	0.0019
PS1753	whole rock	138	184	2.18	0.743524	0.0007
PS1754	garnet 250-500 µm	0.89	0.55	4.69	0.761833	0.0320
PS1755	Epidote	7.98	1415	0.0163	0.718856	0.0007
PS1756	garnet 125-250 µm	1.55	1.31	3.44	0.750976	0.0260
131a (meta-pegmatite; 429.0 ± 2.8 Ma; Sr_i = 0.720461 ± 0.00036; MSWD = 1.8; n = 7)						
PS1965	wm < 355 µm	400	6.31	206	1.968042	0.0021
PS1906	Apatite	1.24	57.6	0.0625	0.720840	0.0009
PS1907	wm 1* (5 mm)	443	6.71	216	2.027034	0.0040
PS1908	Zoisite	60.9	206	0.855	0.725735	0.0017
PS1909	feldspar 1* (2 mm)	316	54.3	17.0	0.826137	0.0012
PS1910	feldspar <355 µm	84.0	30.9	7.92	0.769147	0.0014
PS1911	wm 2* (7 mm)	467	3.76	458	3.503252	0.0043
MF3 (felsic gneiss; 425.7 ± 4.3 Ma; Sr_i = 0.72951 ± 0.00011; MSWD = 1.05, n = 4)						
PS1913	biotite 500-250 µm	302	8.28	113	1.415731	0.0018
PS1914	biotite 250-90 µm	344	5.44	206	1.971942	0.0012
PS1915	qtz-feldspar <355 µm	17.0	50.8	0.969	0.735354	0.0006
PS1918	feldspar single crystal	67.7	124	1.59	0.739226	0.0040
MF4 (mylonite; 419 ± 21 Ma; Sr_i = 0.7320 ± 0.0025; MSWD = 80; n = 9 (excl. biotite))						
433.7 ± 4.5 Ma; Sr_i = 0.732050 ± 0.00038; MSWD = 2.3; n = 3 (plag + 2 big wm)						
PS1924	wm >500 µm	314	78.8	11.6	0.804354	0.0017
PS1848	wm 2000-500 µm	288	98.3	8.53	0.784328	0.0010
PS1852	plagioclase	11.4	354	0.0928	0.732624	0.0009
PS1923	wm 160-90 µm (b)	173	66.7	7.55	0.776004	0.0044
PS1849	wm 355-250 µm	235	67.5	10.2	0.791990	0.0071
PS1853	apatite	3.41	267	0.037	0.732859	0.0022
PS1850	wm 250-160 µm	227	64.7	10.2	0.792398	0.0020
PS2071	wm 500-355 µm	274	74.1	10.8	0.795117	0.0025
PS1851	wm 160-90 µm (a)	166	66.9	7.22	0.773494	0.0062
PS1855	biotite 160-90 µm	268	20.0	39.6	0.967730	0.0054
VAK 1 (pegmatitic felsic vein; 433.2 ± 4.8 Ma; Sr_i = 0.713405 ± 0.000035; MSWD = 2.5; n = 3)						
PS1838	plagioclase*	1.56	1742	0.0026	0.713421	0.0018
PS1903	white mica I*	304	445	1.98	0.725702	0.0016
PS1922	white mica II*	302	481	1.82	0.724554	0.0020

An uncertainty of ±1.5% is assigned to Rb/Sr ratios. wm, white mica; qtz, quartz. Asterisk (*) indicates that single, mm-sized, undeformed crystals were analyzed.

Table DR3.2: Detailed Sm-Nd isotope data.

Sample no. Analysis no.	Material	Sm (ppm)	Nd (ppm)	$^{147}Sm/^{144}Nd$	$^{143}Nd/^{144}Nd$	$^{143}Nd/^{144}Nd$ $2\sigma_m$ [%]
155a (mylonitic micaschist; 462.0 ± 3.5 Ma; Nd_i = 0.511438 ± 0.000011; MSWD = 0.68; n = 5)						
PS1753	whole rock	5.97	31.5	0.1144	0.511787	0.0009
PS1754	garnet 250-500 µm	1.01	0.594	1.029	0.514552	0.0015
PS1756	garnet 125-250 µm	0.709	0.574	0.7463	0.513699	0.0012
PS1919	apatite	26.5	66.8	0.2398	0.512153	0.0011
PS1920	feldspar	0.421	1.94	0.1312	0.511839	0.0025

An uncertainty of ±0.5% (apatite analysis: 1%) is assigned to Sm/Nd ratios.